


RESEARCH

Open Access



Resting state fMRI connectivity is sensitive to laminar connectional architecture in the human brain

Gopikrishna Deshpande^{1,2,3,4,5,6,7*} , Yun Wang^{1,8} and Jennifer Robinson^{1,2,3,4}

Abstract

Previous invasive studies indicate that human neocortical graymatter contains cytoarchitectonically distinct layers, with notable differences in their structural connectivity with the rest of the brain. Given recent improvements in the spatial resolution of anatomical and functional magnetic resonance imaging (fMRI), we hypothesize that resting state functional connectivity (FC) derived from fMRI is sensitive to layer-specific thalamo-cortical and cortico-cortical microcircuits. Using sub-millimeter resting state fMRI data obtained at 7 T, we found that: (1) FC between the entire thalamus and cortical layers I and VI was significantly stronger than between the thalamus and other layers. Furthermore, FC between somatosensory thalamus (ventral posterolateral nucleus, VPL) and layers IV, VI of the primary somatosensory cortex were stronger than with other layers; (2) Inter-hemispheric cortico-cortical FC between homologous regions in superficial layers (layers I–III) was stronger compared to deep layers (layers V–VI). These findings are in agreement with structural connections inferred from previous invasive studies that showed that: (i) M-type neurons in the entire thalamus project to layer-I; (ii) Pyramidal neurons in layer-VI target all thalamic nuclei, (iii) C-type neurons in the VPL project to layer-IV and receive inputs from layer-VI of the primary somatosensory cortex, and (iv) 80% of collosal projecting neurons between homologous cortical regions connect superficial layers. Our results demonstrate for the first time that resting state fMRI is sensitive to structural connections between cortical layers (previously inferred through invasive studies), specifically in thalamo-cortical and cortico-cortical networks.

Keywords: Cortical layers, HRF, Functional connectivity, Resting state fMRI, Blind deconvolution

1 Introduction

The most distinct feature of the mammalian cerebral cortex is its laminar structure, comprised of cortical columns. A cortical column is a unit of complex information processing. It consists of processing chains that overlap, linking multiple inputs to multiple other outputs [1]. A single column of cerebral cortical gray matter normally has six layers. Different layers in the column have distinct distribution and types of neurons as well as separate connections with other cortical and subcortical regions. Our

knowledge about cortical laminar-specific connections is mostly derived from invasive studies including histology, anatomical tract tracing, electrophysiology, and lesion methods [2–7], given that non-invasive modalities, such as magnetic resonance imaging (MRI), both anatomical and functional, have typically lacked the resolution to resolve layer-specific differences.

However, recent developments in ultra-high field functional MRI (fMRI) make it feasible to examine the blood oxygen level dependent (BOLD) signal from cortical and subcortical regions with sub-millimeter resolution. With such resolution, cortical layers can be resolved reasonably, although some amount of partial voluming still exists. In addition, reliable methods have been developed to obtain cortical parcellation in the native

*Correspondence: gopi@auburn.edu

¹ AU MRI Research Center, Department of Electrical & Computer Engineering, Auburn University, 560 Devall Dr, Suite 266D, Auburn, AL 36849, USA

Full list of author information is available at the end of the article

space of individual subjects [8–12]. In the recent past, laminar fMRI studies have investigated the spatial sensitivity of high-field fMRI to the neuronal response at the sub-millimeter level [12–21], primarily using activation paradigms [13, 15, 18, 19, 21–23]. The sensitivity of laminar fMRI has enabled us to understand the columnar profile of cortical activation at a finer spatial scale in the cerebral cortex. However, these investigations were only in the context of laminar fMRI activation (not resting state) within specific brain regions for specific stimuli (example: primary visual cortex with visual stimuli). In addition, previous results were most often achieved with partial brain coverage at ultra-high fields (7 T for humans and >7 T in case of animal studies) unlike whole brain coverage used in conventional resting state fMRI studies.

One popular noninvasive method of analyzing cortical circuits at the voxel level is functional connectivity based on resting state fMRI [24]. Resting state functional connectivity (FC) has been shown to be sensitive to alterations in neural circuits in various mental disorders [25–30] as well as correlated with behavioral performance in healthy individuals [31–33]. Recent literature employing resting state fMRI based characterization of the human brain's functional connectome suggests that resting state fMRI is grounded in underlying anatomical connections [34–37]. For example, simulations have shown that spatially distinct functional networks emerge in resting state data when they are constrained by the structural connectome [38, 39]. The close correspondence between functional and structural connectivity has also been confirmed with fMRI and diffusion tensor imaging (DTI) data [40]. This has been further confirmed in case reports of deficient inter-hemispheric functional connectivity in subjects with complete agenesis of the corpus callosum [41]. However, it is noteworthy that resting state functional connectivity can be sensitive to multi-synaptic interactions, and hence, regions that are not directly connected structurally could still be functionally connected. These data suggest that if two regions have a direct structural connection, then they should also be functionally connected, but the opposite may not be true. Consequently, one could expect a strong functional connection between regions that are also directly connected structurally. In this work, our objective is to extend this concept from mesoscale connections between brain regions to rather microscale connections between different cortical layers in these regions. Attempts to do so have been scarce in the literature. Below, we present previous attempts in this direction. Layer-specific connections between the primary visual cortex layers II/III and middle temporal area layer IV were detected with high-resolution resting state fMRI through functional connectivity analysis [20]. The default

mode network under resting state was clearly seen across six layers by seed-based functional connectivity analysis after removing depth-dependent physiological noise [42]. In addition, a recent study showed the existence of temporal correlation of resting state hemodynamic signals derived from optical imaging at sub-millimeter columnar scale in the visual cortex [43]. These studies suggest that functional connectivity could be a potentially useful method to investigate the laminar connective architecture at the functional level. However, it is yet unclear whether resting state functional connectivity (FC) is in fact stronger along structural pathways that connect different layers of brain regions compared to say, other possible connections between layers that do not have a direct structural projection between them. While this question has been addressed at the meso-scale voxel level, it has not been investigated at the micro-scale layer level. To test these possibilities, many technical challenges need to be surmounted as we discuss below, to provide motivation for the methodological choices we have made.

The major limitation of fMRI is that it is an indirect measure of neural activity, because it measures changes in blood oxygenation level that is modulated by the local vascular distribution (vessel size) and the activation-induced hemodynamic changes [21]. The BOLD fMRI signal can be modeled as the result of the convolution of a latent neural response and the hemodynamic response function (HRF). At the voxel level, the HRF varies across brain regions as well as across individuals [44, 45]. Some animal and human MRI studies at high field have shown that the response height and time-to-peak (TTP) of the HRF varies with cortical depth [18, 46–50]. It was shown that the deeper layers have faster and narrower hemodynamic response compared to the superficial layers. In addition, at the laminar level, gradient-echo BOLD signals have relatively poor laminar specificity, because they are more sensitive to larger vessels [51]. However, a recent investigation of the spatial point spread function (PSF) for the BOLD response showed that the laminar PSF of the gradient-echo BOLD signal had a “flat-tail” characteristic across layers, with the tail running to the pial surface [52]. This indicates that lower layers contribute signal to any given layer in gradient-echo BOLD. While spin echo BOLD may provide better spatial laminar specificity, one may lose sensitivity to the BOLD effect when using spin echo. Investigations into the laminar specificity of BOLD as well as HRF variability across cortical layers have invariably used task-based paradigms and cannot be readily generalized to resting state given that neurovascular coupling likely operates under a different regime in resting state (see extension of Buxton's balloon model to resting state conditions [53]).

Many studies have characterized the effect of HRF variability across regions and subjects [45, 54], as well as the impact of HRF variability across layers [18, 46–50]. However, all of these studies investigated the impact of HRF variability in the context of detecting activation (and not in the context of characterizing functional connectivity). Furthermore, inter-subject and spatial variability of the HRF could potentially give rise to a scenario, wherein the BOLD fMRI time series from any given two regions are synchronized, while the underlying neural response is not, thus giving high correlation between BOLD signals, while the true correlation between latent neural variables may be low. The opposite scenario, wherein the underlying neuronal variables are synchronized, while the BOLD fMRI time series are not, is also equally possible (see Additional file 1: Fig. S1 for illustration of these scenarios). Therefore, we need to extract the underlying latent neural response to get reliable estimates of FC between layers of different regions. The readers are referred to Rangaprakash et al. for more details on the effects of HRF variability on functional connectivity [55].

In this study, we applied a surface-based laminar analysis pipeline available in FreeSurfer (<https://surfer.nmr.mgh.harvard.edu/>) to process high-resolution anatomical data with a 0.6 mm isotropic resolution and to delineate the six layers of the cortex [56, 57]. To investigate whether FC is sensitive to layer-specific connective architecture, we examined this aspect with high-resolution resting state fMRI data (voxels with 0.85 mm in-plane resolution) obtained at 7 T. A simple blind deconvolution technique [58] was used to obtain the latent neural signals for each layer. Specifically, we tested the following hypotheses regarding thalamo-cortical and cortico-cortical layer-specific microcircuits derived from previous invasive anatomical studies (Fig. 1): (1) FC between the entire thalamus and cortical layers I and VI must be significantly greater than between the whole thalamus and other layers. This follows from evidence in rat brain tracing studies which show that regions across the cortex receive inputs to layer I from M-type thalamic neurons distributed in most thalamic nuclei [59–64]. In addition, pyramidal neurons in layer-VI are known to target all thalamic nuclei. Furthermore, FC between somatosensory thalamus (ventral posterolateral nucleus, VPL) and layers IV and VI of the primary somatosensory cortex (S1), must be stronger than other layers. This follows from the well-known C-type thalamic neurons in VPL that primarily target layer IV in the primary somatosensory cortex, and then corticothalamic pyramidal neurons in layer VI are known to project back to C-type thalamic neurons in VPL [65, 66], (2) inter-hemispheric cortico-cortical FC (i.e., between the left and right brain regions of the same area) in superficial layers (layers I–III) must be higher

compared to deep layers (layers V–VI). This follows from evidence in rodents that 80% of the cell bodies of those callosal projecting neurons are distributed in layer II and layer III, with only 20% in layers V and VI [67, 68]. Other studies have claimed that layers I through III are the main target of inter-hemispheric cortico-cortical afferents, while some suggest that layer III is the main source of cortico-cortical efferents [69–71]. Taken together, it makes sense to hypothesize higher cortico-cortical FC in superficial layers compared to deeper layers.

We found that resting state functional connectivity at the laminar level, to a great extent, were in sync with the hypotheses stated above. To the best of our knowledge, we are the first to show that fine-grained layer-specific thalamo-cortical and cortico-cortical anatomical connections between cortical layers are reflected by stronger resting state functional connectivity in these pathways.

2 Results

2.1 Surface-based laminar analysis and blind deconvolution

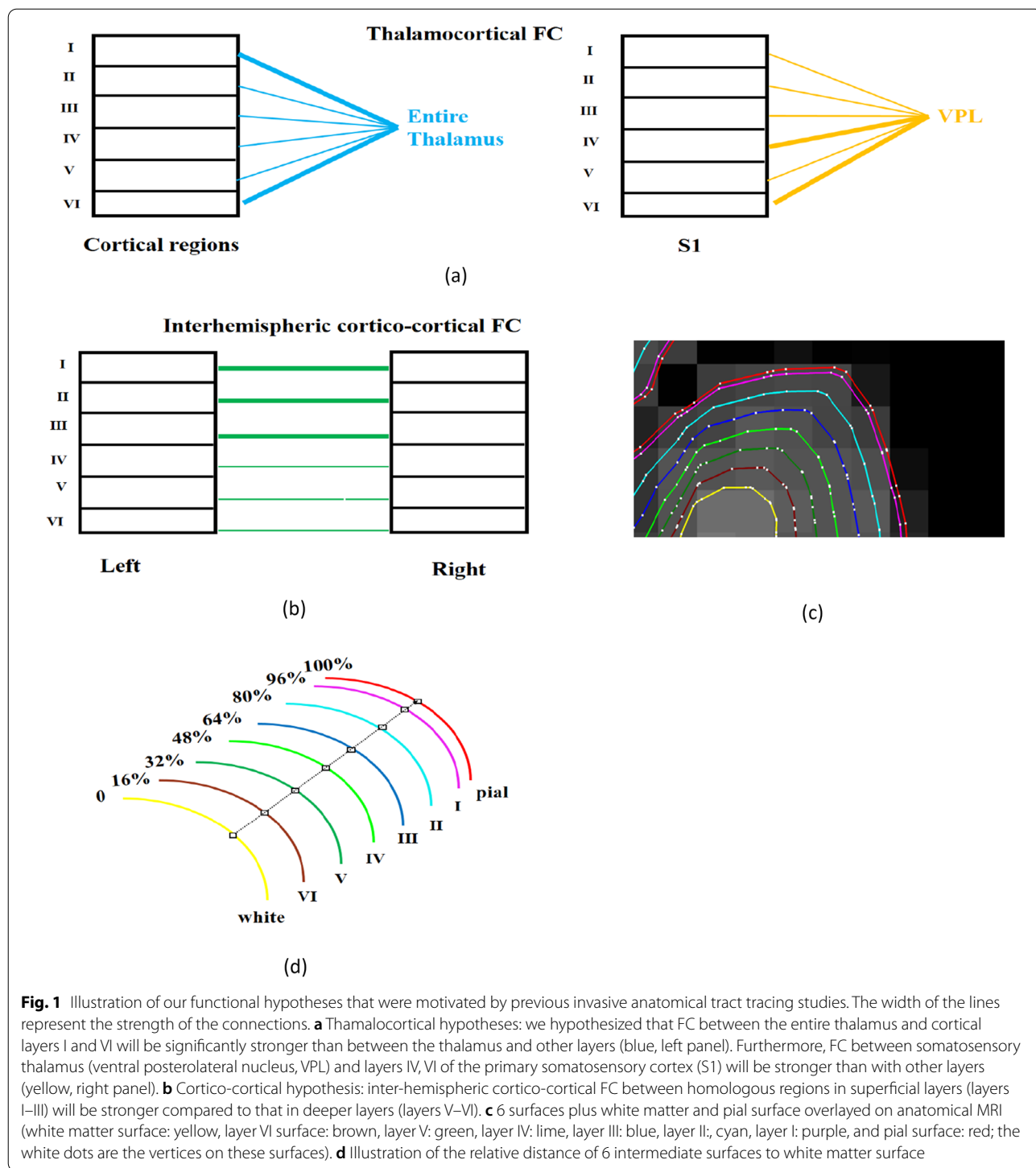
We employed a surface-based laminar analysis pipeline to extract vertex-based resting state fMRI time series for 68 cortical regions separately from six layers of the neocortex (Fig. 2). Then, we performed vertex-by-vertex blind deconvolution [58] to get each vertex's latent neural response and HRF. Please refer to the methods section for further details on these analyses.

2.2 Functional connectivity across cortical regions between layers

With each vertex's latent neural response, we calculated the mean time series for 68 regions of interest in each layer. To investigate global trends, we estimated the mean Pearson's correlation between the 68 ROIs (using latent neural signals) in a given layer and those in all layers. The mean correlation did not show any significant difference between layers (Fig. 3). This demonstrates that global connectivity differences between layers were absent.

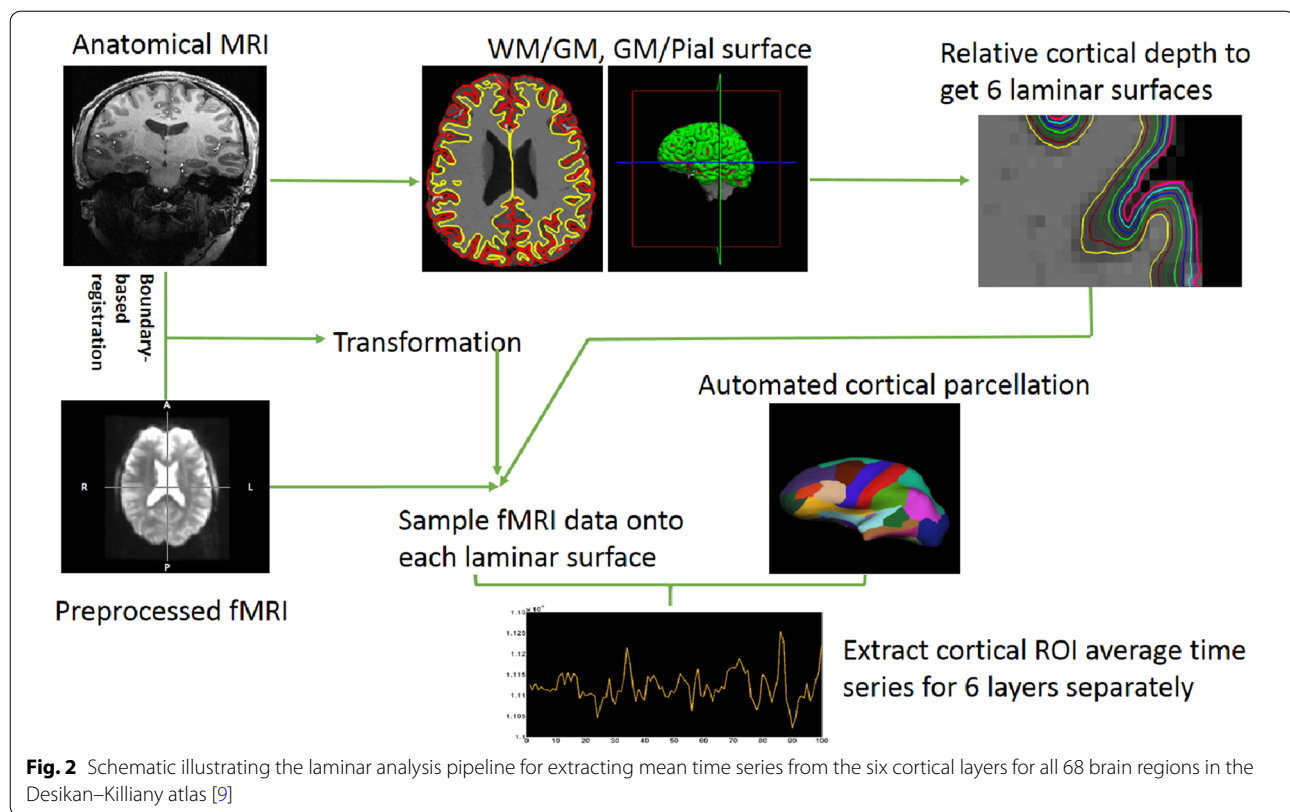
2.3 Hypotheses testing before deconvolution

To test the thalamocortical hypothesis, we computed the Pearson's correlation between the mean time series extracted from 68 ROIs in each layer with the mean time series extracted from the entire thalamus. For testing the specific VPL ↔ S1 connectivity hypothesis, the Pearson's correlation between the mean time series from primary somatosensory cortex (S1) and the VPL were computed. For testing the cortico-cortical hypothesis, we estimated the mean inter-hemispheric correlations only between homologous regions in each layer. The functional connectivity pattern for thalamo-cortical connections showed that the mean Pearson's



correlation between layer I and the entire thalamus was strongest across the cortex (Fig. 4a), and was significantly (FDR corrected $p < 0.05$) greater than the correlation between the thalamus and layers II–VI. Although layer IV showed a trend to be more strongly connected to the thalamus, it did not reach significance.

In contrast, VPL ↔ S1 connectivity was significantly stronger in layer IV than in layers I, V, and VI (Fig. 4b). We then examined the inter-hemispheric cortico-cortical connections for all 68 cortical regions for each layer (i.e., between the left and right brain regions of the same area). We found that the inter-hemispheric



cortico-cortical mean correlation for layer III was significantly greater than layer VI (Fig. 4c).

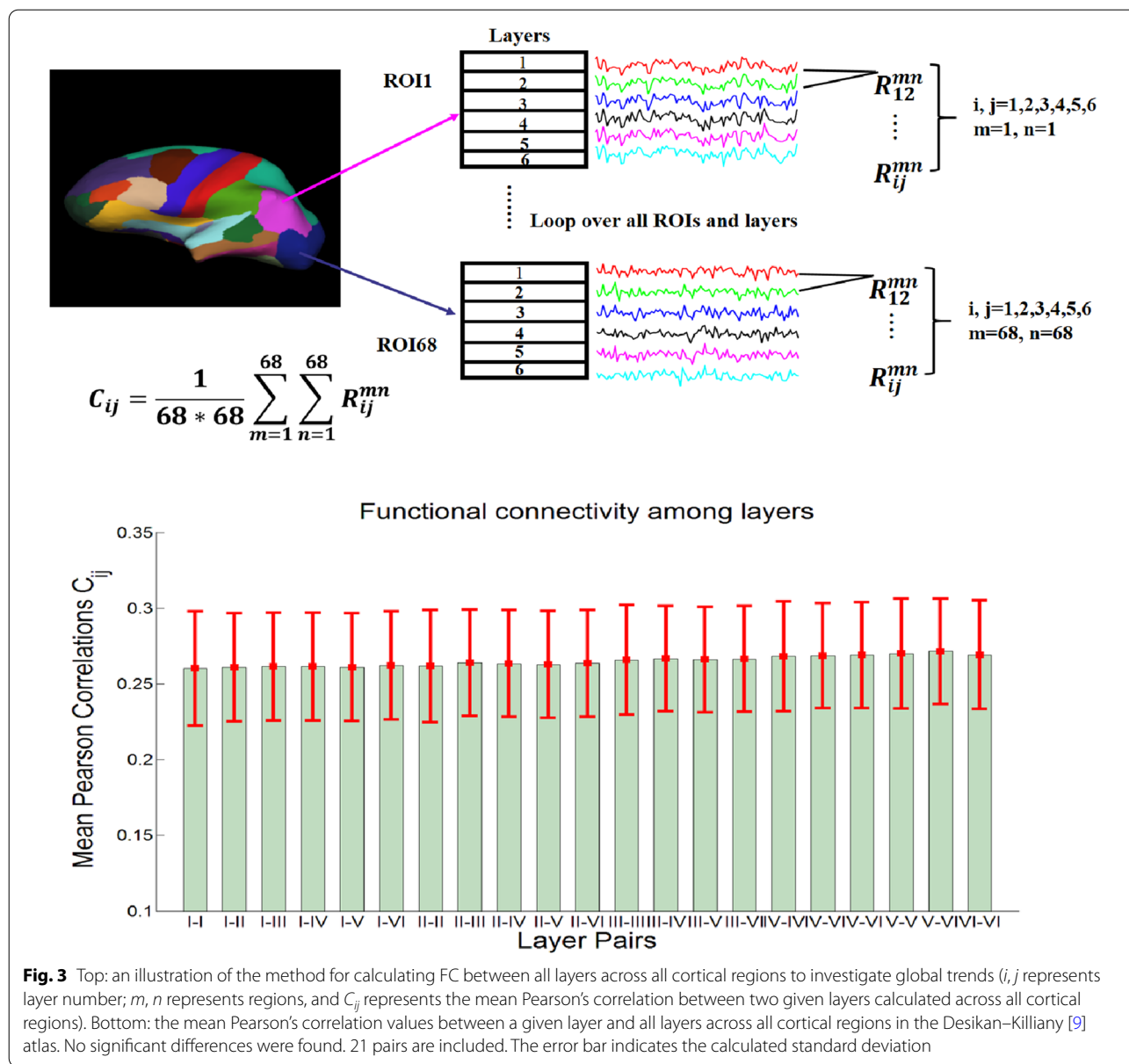
2.4 Laminar HRF differences

The hemodynamic response could be different between regions across subjects and it has been previously shown that this might impact the estimates of connectivity obtained between such regions [44, 54]. To assess the laminar variability of the HRF and recover the neural response, we performed blind deconvolution before functional connectivity analysis. To assess the effect of deconvolution, we compared the shape of region-specific HRFs across six layers (Fig. 5). Three parameters of region-specific HRFs we examined were response height, time-to-peak, and full-width at half-max (FWHM). The means and standard deviations of the three parameters were calculated separately for each layer across all subjects. As an illustration, we show the region-specific HRF results for left orbitofrontal cortex (Fig. 5a–d) and primary somatosensory cortex (Fig. 5e–h), which are two of the 68 parcellation regions.

After one-way analysis of variance (ANOVA) for response height ($p=0.0469$), time-to-peak ($p=0.0026$), and FWHM ($p=0.0268$) of region-specific HRF separately, we found response height as well as time to peak and FWHM were significantly different across the layers

($p<0.05$ FDR corrected) for left orbitofrontal cortex. In addition, the three parameters were distinct across layers for left primary somatosensory cortex as well ($p=0.0035$ for response height, $p=0.0014$ for time-to-peak, and $p=0.0312$ for FWHM). Furthermore, multiple comparison of means in one-way ANOVA was employed for each parameter. Here, for the left orbitofrontal cortex, we found that the response height and FWHM of layer I was significantly ($p<0.05$ corrected) larger than for layer VI, and time to peak of layers I, II, and III was significantly ($p<0.05$ corrected) larger than layer VI. For the primary somatosensory cortex, we found that the response height and time to peak of layer I were significantly ($p<0.05$ corrected) larger than for layers III–VI, and at the same time, the response height and time to peak of layer VI were significantly smaller ($p<0.05$ corrected) than layer II. Moreover, FWHM of layer I was significantly ($p<0.05$ corrected) wider than layer VI.

To investigate whether this is a general fact for all region-specific laminar HRFs, we performed similar analyses for all other 66 regions and summarized the results in Fig. 6. 66 out of 68 regions had significant difference ($p<0.05$ corrected) across the layers for the response height, 62 out of 68 regions for time to peak, and 36 regions for FWHM. In summary, the HRF varies across cortical layers in many brain regions and it is



necessary to recover the latent neural signal at each layer before performing connectivity analysis.

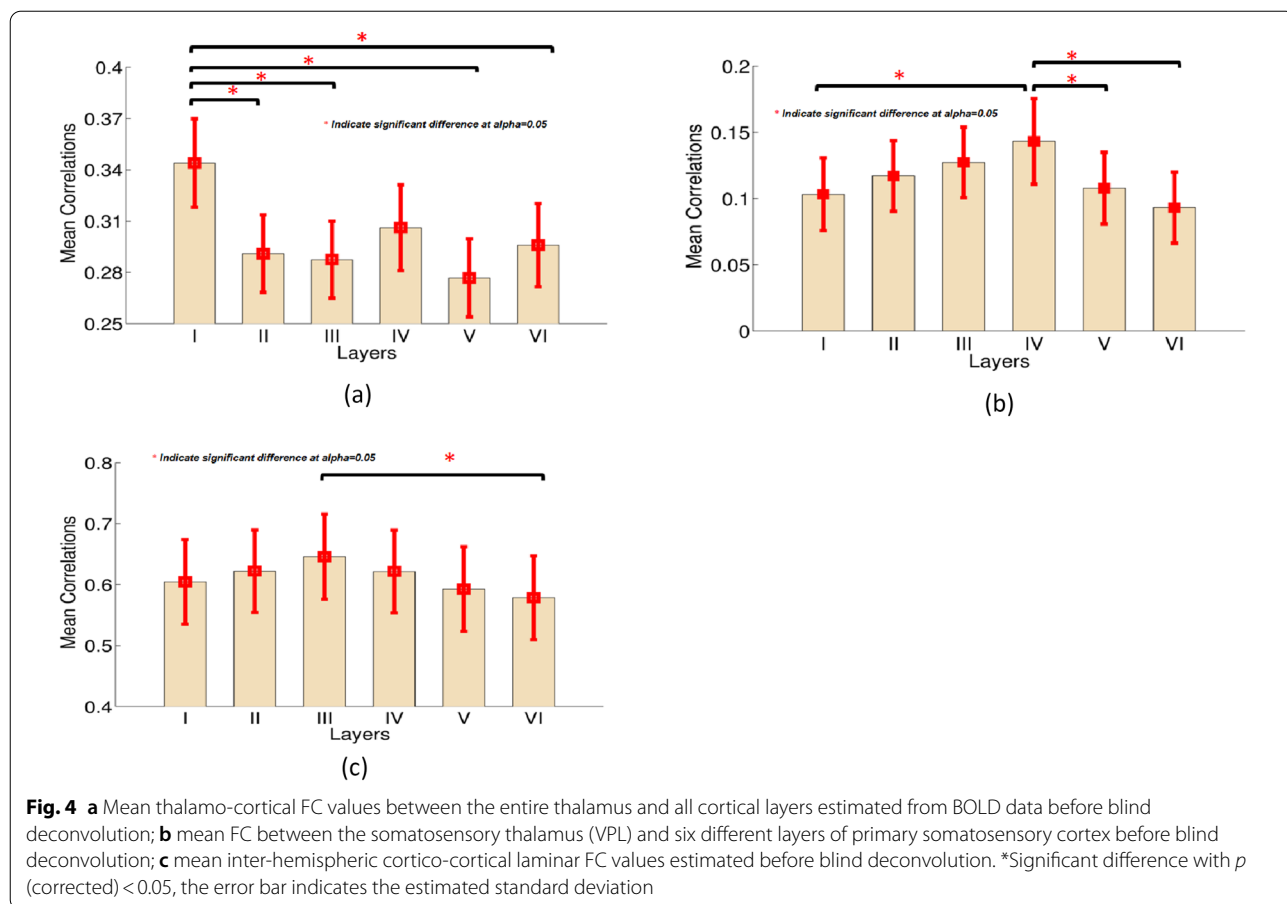
2.5 Individual-level FC difference before and after deconvolution

We estimated individual-level mean connectivity values of all possible connectivity paths between the 68 ROIs and the results for all 20 subjects, obtained with both deconvolved and non-deconvolved data, are shown in Fig. 7. The differences in connectivity due to deconvolution are plotted at the bottom part of Fig. 7, showing the magnitude of change caused by HRF variability in each subject. The group average non-deconvolved FC value

was 0.033 higher than deconvolved FC value. A paired t test between non-deconvolved FC and deconvolved FC returned a high statistical significance for all paths ($p=0.0012$).

2.6 Hypotheses testing after deconvolution

Results obtained after deconvolution, i.e., those estimated from latent neural signals, were more in sync with our hypotheses. As we can see from Fig. 8a, FC between the entire thalamus and Layer I across the cortex was significantly greater than the FC between the entire thalamus and layers II–VI (FDR corrected $p < 0.05$). In addition, FC between the entire thalamus and Layer VI was



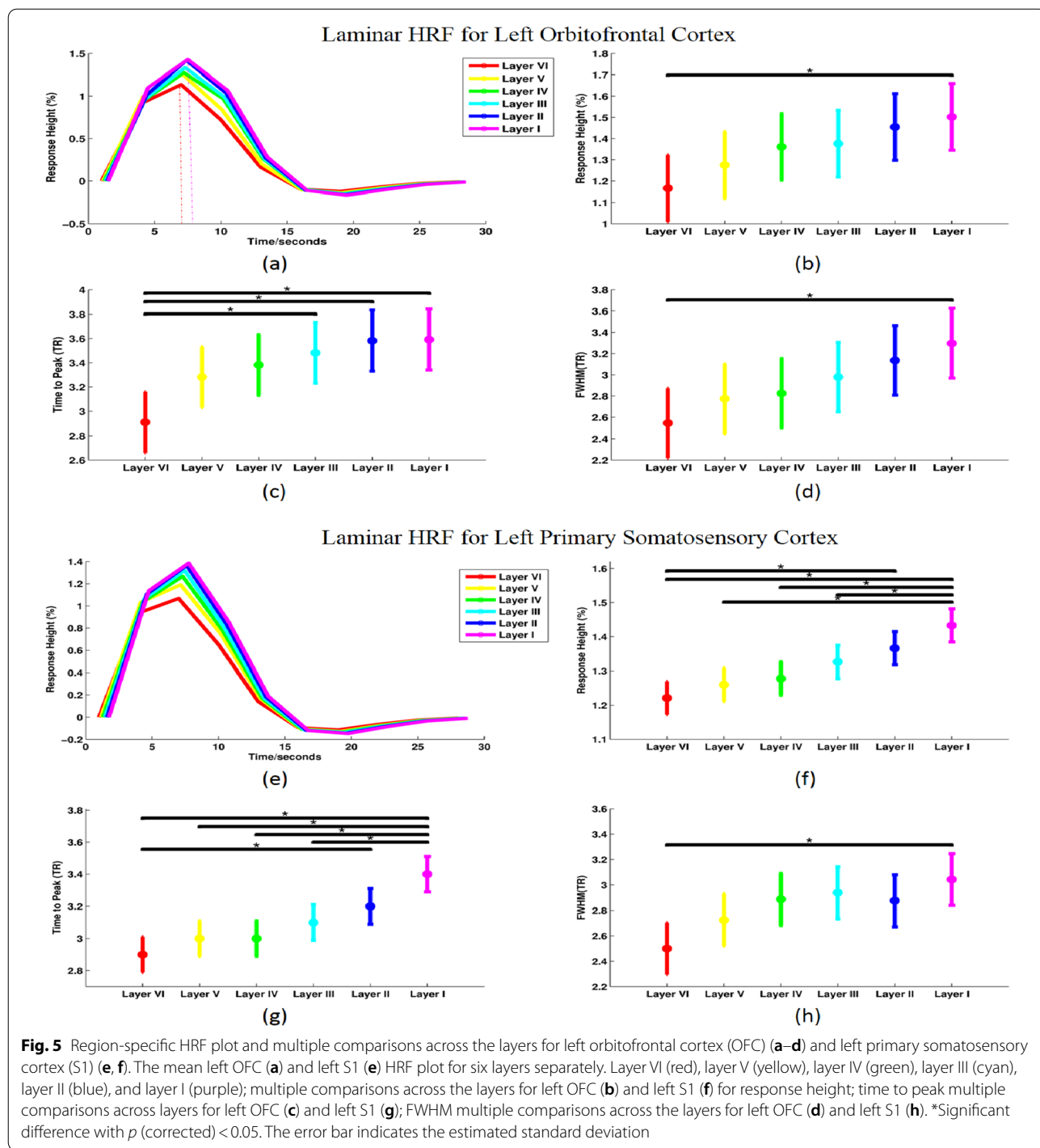
significantly higher than FC between the entire thalamus and layers II, III, and V. In contrast, the FC between sensory core thalamus (VPL) and layers IV, VI of S1 was significantly stronger than between VPL and layers I, II, III, and V (Fig. 8b).

Finally, we examined the inter-hemispheric cortico-cortical FCs for each layer (i.e., between the left and right brain regions of the same area) and compared the FC results before deconvolution (Fig. 4c) with FC results after deconvolution (Fig. 8c). Before deconvolution, only the inter-hemispheric cortico-cortical FCs for layer III were significantly greater than layer VI (Fig. 4c). However, after deconvolution, FCs between homologous regions in layers I–III were significantly greater than in layers IV–VI (Fig. 8c). Generally speaking, the inter-hemispheric mean correlations in superficial layers were higher compared to those deeper layers [71].

3 Discussion

In this study, we tested hypotheses involving thalamo-cortical and cortico-cortical layers specific microcircuits derived from previous invasive anatomical studies. The thalamo-cortical hypothesis is that FC between the

entire thalamus and cortical layers I and VI must be significantly greater than that between the thalamus and other layers. This hypothesis is based on the fact that the regions across the cortex receive inputs to layer I from M-type thalamic neurons distributed in most nuclei of the thalamus and receive cortico-thalamic radiations from layer VI of the cortex [59–64]. Accordingly, we found that FC (estimated from latent neural variables) between the entire thalamus and layer I was indeed significantly greater than between the thalamus and layers II–VI, and FC between the thalamus and layer VI was higher than between the thalamus and layers II, III, and V. In addition, we found the FC between the sensory core thalamus (i.e., VPL) and layers IV and VI of the primary somatosensory cortex, were higher than other layers. This follows from the fact that C-type thalamic neurons in VPL primarily target layer IV in the primary somatosensory cortex, and then corticothalamic pyramidal neurons in layer VI project back to C-type thalamic neurons in VPL [65, 66]. To a large extent, the results confirmed our hypotheses. The cortico-cortical hypothesis is that inter-hemispheric cortico-cortical FC in superficial layers (layers I–III) must be higher compared to deep



layers (layers V–VI) following evidence in rodents that 80% of the cell bodies of those callosal projecting neurons are distributed in layer II and layer III, with only 20% in layers V and VI [67–71]. Our results suggested that the inter-hemispheric FC was significantly higher in superficial layers than deeper layers. To our knowledge, this is the very first study to investigate the sensitivity of resting

state fMRI connectivity at sub-millimeter spatial scale to the connectional architecture at the laminar level.

One common concern in laminar fMRI studies is the large signal amplitude on the pial surface, which could be potentially affected and contaminated by large veins on the cortical surface, or partial volume effects from large voxel sizes. Different methods have been employed to

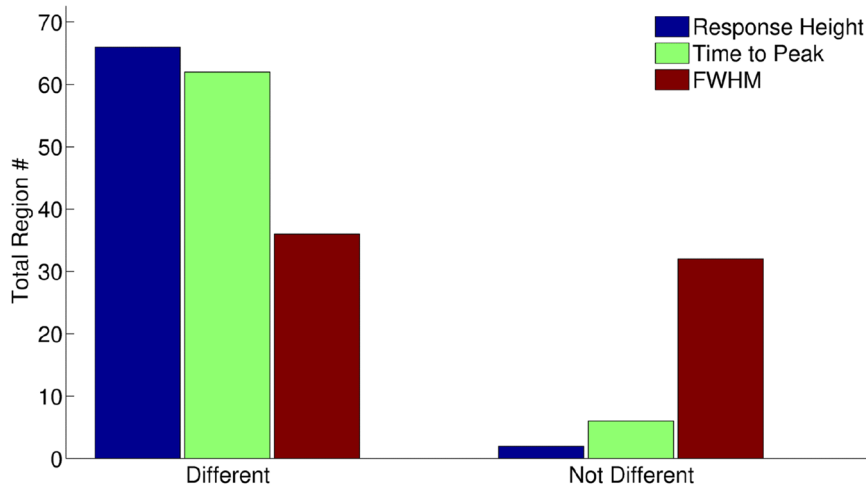


Fig. 6 Summary of one-way ANOVA analysis performed on HRF parameters (response height, time to peak, and FWHM) for 68 regions. 66 out of 68 region had significant difference across the layers for the response height, 62 out of 68 regions for time to peak, and 36 regions for FWHM at p (corrected) < 0.05

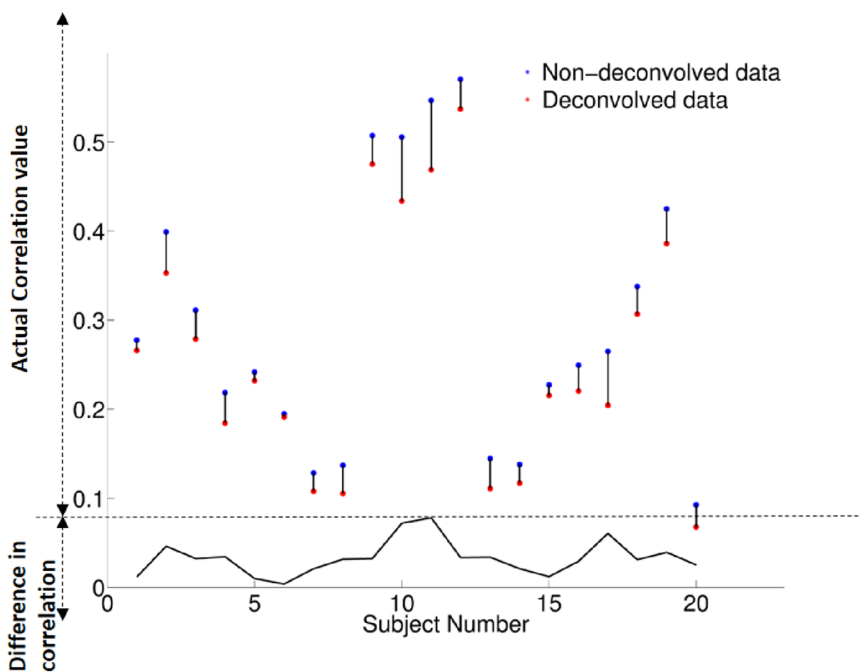
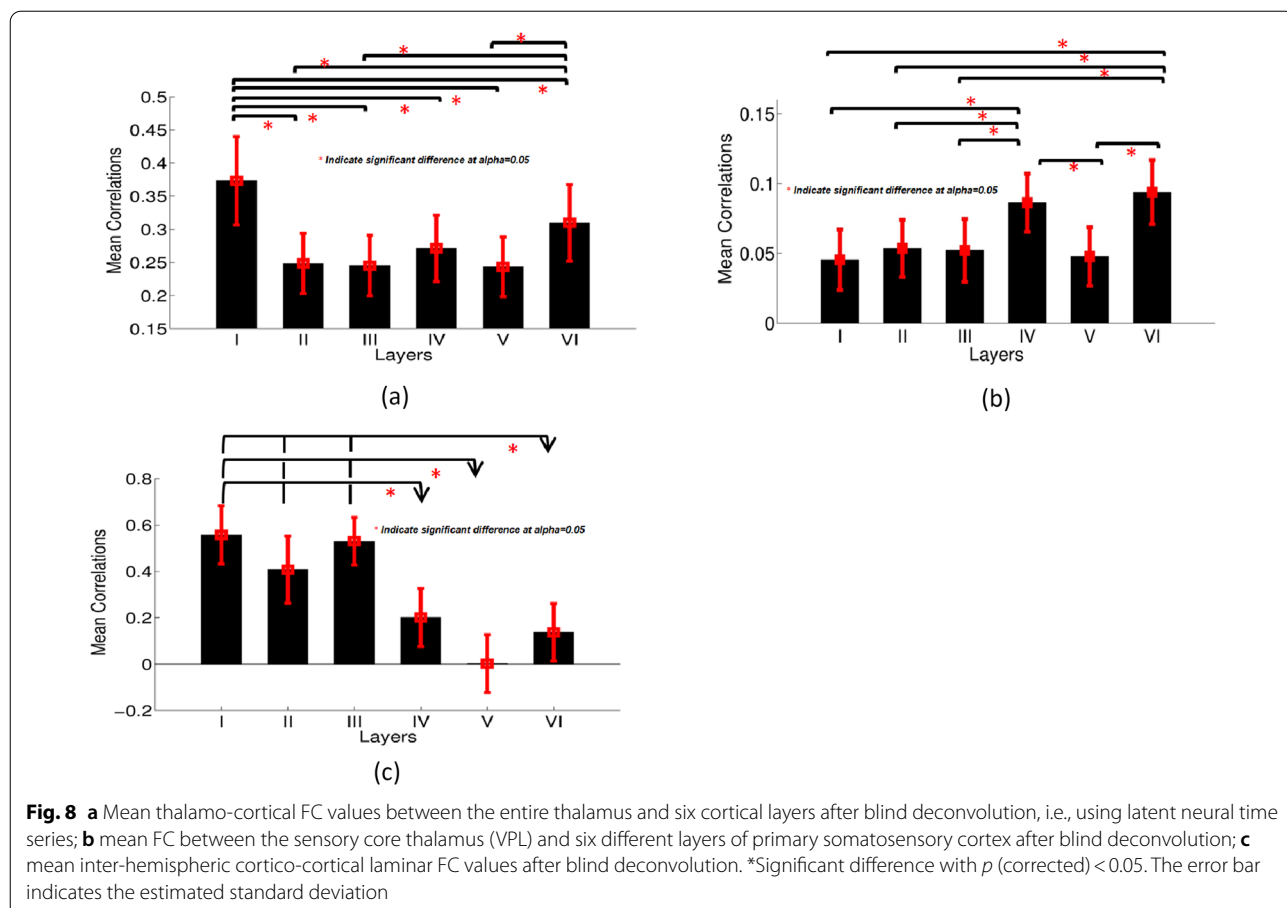


Fig. 7 Comparison of the individual-level average FC values before and after deconvolution for all paths. Blue represents FC values with non-deconvolved data, and red for FC values after deconvolution

resolve the large vein problem. Simply avoiding the first layer compartment is the easiest way [21]. Indeed, if we did consider our hypotheses by excluding the first layer, they would be confirmed by our results. Another alternative approach is restricting the laminar analysis to strongly activated clusters in each subject [18]. A novel

pial vein pattern analysis by optical imaging was suggested by Chen et al. to remove voxels associated with large veins, and the vein-free fMRI exhibited clear laminar specificity [13]. However, around 40% of activated voxels in the primary visual cortex was excluded for this study. In addition, optical imaging technique used by



Chen et al. was invasive, and hence is not suitable for human studies. In this study, we approached this issue in terms of HRF differences across layers. We reasoned that any differences between BOLD signals across layers that have a vascular origin, must be reduced or eliminated if voxel (or vertex-specific) HRF was deconvolved from the BOLD data and connectivity estimation was performed in the latent neural space.

To investigate the variability of HRF across layers, we employed a simple but powerful blind deconvolution technique to recover the latent neural signal at each vertex. Our results showed that all three parameters of region-specific laminar HRF (response height, time-to-peak, and FWHM) varied in reference to cortical depths, and were significantly greater in superficial layers than deeper layers. This finding matches findings from previous HRF studies in animals. Tian et al. found both the onset of the BOLD response and the initial dip rely on cortical depth, and the fastest response was in deeper layers within the rat primary somatosensory cortex [49]. In addition, Yu et al. showed the onsets at different layers coincided with the neural inputs with line-scanning fMRI both in rat somatosensory cortex and motor cortex

[47]. We have demonstrated that this is a general fact for almost all cortical regions. The comparison of functional connectivity before and after deconvolution showed the importance and necessity of recovering latent neural signals before any resting state functional connectivity analysis is performed at the laminar level. The functional connectivity post-deconvolution in the latent neural space aligned more closely with the underlying anatomical connections compared to FC obtained on BOLD data.

3.1 Limitations and future work

There are a few limitations of present study, which need to be addressed in future layer-specific fMRI functional connectivity related research. First, different methods exist for identifying different cortical lamina from MRI data. The method we employed was to construct laminar profiles, which keeps a relatively fixed distance to the cortical boundaries (Fig. 1), the so-called equidistant laminae [18, 72, 73]. An alternate approach is the equipotentials method, wherein the equipotentials are computed between the inner white matter surface and pial surface with the Laplace equation, and then the cortical profiles can be constructed along the gradients [74].

However, the drawback with this approach is that the Laplacian equation may not match the anatomical layers observed from high-resolution MRI [75]. Recently a new model called equal-volume model for identifying cortical laminae was proposed by Waehnert et al. [75], and they claimed that it provides a better fit to observed cortical layering. In future, studies must compare the three different models for how well functional connectivity derived from layers constructed by them match the underlying anatomical predictions.

Second, the spatial laminar point spread function (SL-PSF) of the BOLD response presents a fundamental stumbling block for gaining laminar specificity in fMRI data. Lower layers always contribute signal to the upper layers, because the intracortical veins (ICV) are perpendicular to the surface, and the draining blood flows along the ICV into pial veins on the pial surface [52]. The interpolation-averaging method, wherein the fMRI volume is interpolated at certain cortical depths and the surface profiles are averaged, has been proposed for addressing this issue [18, 21, 22], but a more precise method to extract laminar signals is needed. As we briefly mentioned in the introduction, this is especially true for gradient echo EPI based fMRI which has a flatter PSF compared to spin-echo based EPI. Therefore, future studies may investigate whether spin echo EPI may be better for FC studies at the laminar level, even with the loss of sensitivity in spin echo compared to gradient echo. Recently, an extension of the Friston–Buxton hemodynamic model, which accounts for blood draining effects by coupling local hemodynamics across layers in dynamic causal models of fMRI during visual activation, was reported [14]. However, priors about two parameters controlling blood draining effects (the delay τ_d between the lower and upper layers, and λ_d which represents the strength of the blood draining effect from the lower to the upper layers) need further experimental validation in human resting state studies. Investigations into the laminar specificity of BOLD have invariably used task-based paradigms and cannot be readily generalized to resting state given that neurovascular coupling likely operates under a different regime in resting state (see extension of Buxton's balloon model to resting state conditions [53]). Therefore, further modeling and experimental work is needed in this area, which could potentially lead us to a reliable and accurate laminar time series that will allow a more fine-grained investigation of resting state FC at the laminar level.

Third, the hypotheses we chose to test provide only an initial demonstration of the sensitivity of resting state fMRI functional connectivity to layer-specific functional microcircuits in the human brain. However, further fine-grained investigations are possible. This could involve

specific thalamo-cortical pathways from other thalamic nuclei, specifically in systems that are unique in humans and for which we do not have reliable homologues in animals, and hence are not amenable to invasive investigations. For example, two parallel layer-specific pathways connect language-related thalamic nuclei to layer I and middle layers of Broca's area. The cortico-thalamic radiations from Broca's area in turn originate from cortical layers V and VI. Dysfunction in these pathways are important in aphasic patients with damage to the thalamic nuclei [76]. Our study opens the possibility of characterizing such layer-specific microcircuits, both in healthy and clinical populations, using ultra high field fMRI in the future.

Fourth, it is well recognized that functional connectivity cannot decipher the direction of information flow between regions, where as many anatomical projections which we have based our hypothesis on, are in fact directional in nature. Therefore, the next logical steps would be to test whether directional connectivity models of fMRI such as dynamic causal modeling (DCM) [77] and Granger causality (GC) [78–81] are sensitive to direction-specific anatomical projections at the layer-level.

Fifth, we have used the DK atlas to identify regions of interest given the fact that it is widely used and available as a surface. However, better atlases are available for volume-based analysis, which are less coarse and homogeneous than the DK atlas. Using such an atlas in the surface domain may improve the fidelity of the results.

Sixth, we do acknowledge that there may be regional specificity in the structure–function relationship, but previous evidence suggests that such specificity may be less for thalamo-cortical connections as well as inter-hemispheric connections between homologous regions. In addition, not all cortical regions have six layers. Therefore, it is reasonable to surmise that the broad nature of our hypotheses might have averaged out some effects and decreased their effect sizes. Testing more specific hypotheses in future studies may unravel the full extent of the utility of layer specific FC investigations.

Finally, we employed a gradient echo EPI sequence optimized for SNR and spatial resolution. The sequence used for data acquisition for testing FC-related hypotheses at the laminar level could well be optimized in other ways. This includes using a spin echo sequence and trading sensitivity for a narrow SL-PSF, as well as using a multiband EPI sequence to obtain a shorter TR, possibly at the cost of SNR (but not spatial resolution). One way of increasing the spatial resolution further would be to restrict coverage to regions specifically relevant to the hypothesis being tested, but this would require a custom processing pipeline (other than the one in FreeSurfer) that does not require whole brain coverage. In summary,

our seminal study offers a lot of possibilities for investigating the brain's functional connectome at a more fine-grained laminar spatial scale.

4 Methods

4.1 Data acquisition

Twenty healthy adult subjects (10 males, 10 females; 24.5 ± 3.3 years of age) participated in this study. All subjects provided informed consent, and the experimental protocols were approved by the Auburn University Institutional Review Board. High resolution resting state fMRI data was obtained from twenty healthy individuals using an EPI sequence with the following parameters: 37 slices acquired parallel to the AC-PC line, $0.85 \text{ mm} \times 0.85 \text{ mm} \times 1.5 \text{ mm}$ voxels, TR/TE: 3,000/28 ms, 70° flip angle, base/phase resolution 234/100, A \rightarrow P phase encode direction, iPAT GRAPPA acceleration factor = 3, interleaved acquisition, 100 timepoints. Data were acquired on a Siemens 7 T MAGNETOM outfitted with a 32-channel head coil by Nova Medical (Wilmington, MA). During resting state, the subjects were instructed to keep their head as still as possible, keep their eye open and let their mind wander and not think about anything specific.

A whole-brain high-resolution three-dimensional (3D) MPAGE sequence (256 slices, $0.6 \text{ mm} \times 0.6 \text{ mm} \times 0.6 \text{ mm}$, TR/TE: 2,200/2.8, 7° flip angle, base/phase resolution 384/100%, collected in an ascending fashion, acquisition time = 14:06 min) was used to acquire anatomical data.

4.2 Functional MRI data preprocessing

First five timepoints were discarded from the analysis to allow for MR equilibration. Slicing time correction was applied, and all functional MRI data were motion corrected using rigid body registration using SPM software (<http://www.fil.ion.ucl.ac.uk/spm/>). Next, linear trends were removed from each voxel time series. We also removed nuisance variance in the data by regressing out mean time series from ventricular CSF, white matter, as well as six head motion parameters. Importantly, spatial smoothing and spatial normalization were not performed. Spatial smoothing negates the advantages gained by smaller voxels sizes. In addition, spatial smoothing is employed in traditional general linear model based activation analysis to satisfy the assumptions of random field theory. We did not perform those kinds of analysis and hence found it unnecessary to spatially smooth the data. Next, the Freesurfer analysis pipeline enables individual-specific cortical parcellation from which we extracted the time series used in the analysis. Therefore, we found that spatially normalizing the data into a common space and incurring the costs of blurring and registration errors associated with such a procedure was unnecessary and

may be counter-productive for the small voxel size we had and the type of analysis we planned.

4.3 Surface-based MRI analysis

Cortical surface reconstruction of the cerebral cortex from magnetic resonance images is a major step in the quantitative analysis of the human brain structure. Cortical reconstruction approaches with Freesurfer are optimized for standard resolution ($\sim 1 \text{ mm}$) data. However, in this work, we applied Lüsebrink's method to preprocess high-resolution anatomical MRI data with our original 0.6 mm isotropic resolution using FreeSurfer 6 beta version [82]. The white/gray and gray/CSF interfaces, as well as cortical thickness maps were automatically generated with FreeSurfer (Fig. 1). The surfaces generated by FreeSurfer are represented in the form of triangular meshes, and each triangle has three vertices. In addition, a set of 3D coordinates of these surfaces gives the position of the vertices.

Once we obtained the white matter and pial surfaces, the laminar profiles were delineated within the cortical gray matter. They were constructed at fixed relative distance between the white matter and pial surfaces, determined from cortical thickness [21]. The position of each vertex on intermediate surfaces depends on the position of the corresponding vertex on the white matter surface (Fig. 1). The first intermediate surface was located at 16% of cortical thickness away from the white matter surface, then at 32%, 48%, 64%, 80%, and 96% depths, giving us a total of 6 layers (Fig. 1). In addition, cortical regions defined on the inflated surface were automatically obtained from the Desikan–Killiany (DK) Atlas, including the primary somatosensory cortex [9]. The whole thalamus was identified in MRI volume data using automatic subcortical segmentation proposed by Fischl et al. [83]. We defined the sensory core thalamus (VPL) mask from the Oxford thalamic connectivity atlas [84] in common MNI space, and transformed the mask to each individual's coordinate space.

4.4 Registration of functional MRI to anatomical MRI

To enable the analysis of laminar fMRI, we need to align the fMRI volumes to those intermediate laminar surfaces. Apparently, the gray/white matter boundary in the EPI volume is easily identified automatically. We employed a method called boundary-based registration (BBR) [85]. It identified the interface between gray matter and white matter in the EPI data and then calculated a 12 degrees of freedom affine transformation, which registers the interface in EPI data to the corresponding surface reconstruction from the anatomical data (Fig. 2). After the

registration, the results were visually inspected for each subject and manually edited, if needed [85].

4.5 The extraction of functional MRI data from different layers

The preprocessed fMRI volume data were then transformed onto the six laminar surface reconstructions using the transformation matrix obtained in the previous step above. An average time series was extracted from the whole thalamus. This was done, because our first hypothesis involved the M-type thalamus cells distributed in each nucleus of thalamus [59–64]. Next, time series from each vertex in 34 lateral cortical ROIs in the DK atlas [9] were extracted, separately for left and right hemispheres in each subject. The 68 ROIs' mean time series corresponding to the cortical ROIs were extracted for each of the 6 layers (Fig. 2). The regions in the DK atlas are defined on an inflated surface by manually tracing from the depth of one sulcus to another, thus incorporating the gyrus within. Therefore, unlike volume based ROIs that are affected by the folding pattern of sulci and gyri, the surface-based definition of DK atlas ROIs means that the results are not affected by the gyral and sulcal folding patterns.

4.6 Blind deconvolution

After the time series in the preprocessed functional data were transformed onto the six laminar surface reconstructions, we performed vertex by vertex (a vertex is a point on a triangle surface as explained before, see Fig. 1c) blind deconvolution [58] to get each vertex's latent neural response and HRF.

Hemodynamic deconvolution of the BOLD signal is under the assumption that the relationship between a latent neural signal and the BOLD response can be modeled as a linear and time invariant system, which can be described as follows:

$$y(t) = x(t) \otimes h(t) + e(t) \quad (1)$$

where $y(t)$ denotes the observed BOLD signal, $x(t)$ denotes the underlying latent neural signal and $h(t)$ and $e(t)$ represent the HRF and the noise term in the measurement, respectively. Since the three terms in right side are unobservable quantities, we consider the neuron activity term $x(t)$ as a simple on–off model with series of delta functions $\hat{x}(t)$ as

$$\hat{x}(t) = \sum_{\tau=0}^{\infty} \delta(t - \tau). \quad (2)$$

Note that the delta functions modeling the events exist at random times, which essentially amounts to modeling the resting state data as an event-related paradigm with randomly occurring events. Then the HRF $h(t)$ was fitted using a canonical HRF (two gamma functions) and two derivatives (temporal derivative and dispersion derivative). The parameters of $h(t)$ were allowed to vary for each time series. The approximation $\tilde{x}(t)$ of the latent neural signal can be obtained from the observed data using a Wiener filter as described below:

$$\tilde{x}(t) = d(t) \otimes y(t), \quad (3)$$

where \otimes denotes convolution. Applying Fourier transforms to $h(t)$, $y(t)$, $e(t)$, and $d(t)$, respectively, we get $H(\omega)$, $Y(\omega)$, $E(\omega)$, and $D(\omega)$. $D(\omega)$ can be expressed as follows:

$$D(\omega) = \frac{H^*(\omega)}{|H(\omega)|^2 + |E(\omega)|^2}, \quad (4)$$

where $*$ denotes complex conjugate. The estimate $\tilde{x}(t)$ of the latent neural signals $x(t)$ is then given by

$$\tilde{x}(t) = \mathcal{F}^{-1} \left\{ D(\omega) Y(\omega) \right\} = \mathcal{F}^{-1} \left\{ \frac{H^*(\omega) Y(\omega)}{|H(\omega)|^2 + |E(\omega)|^2} \right\}. \quad (5)$$

In Eq. 5, \mathcal{F}^{-1} is the inverse Fourier transform operator. Since the measurement noise $e(t)$ is assumed to be white, the covariance of the noise term must be 0. For task-related fMRI, the stimulus function provides the prior information about neural activity and a generative model whose inversion corresponds to deconvolution. Here, resting state fMRI is considered as a spontaneous event-related signal, and these events can be reflected by relatively large amplitude BOLD signal peaks [58, 86]. Therefore, the time series from each vertex was evaluated against a given amplitude threshold around the local maximum (threshold was set to 1, since the input time series were normalized) to obtain a set of estimated onsets (the timing of delta functions) for these pseudo-events. To get the delay τ (the delay between the peak of fMRI and the peak of neural signal), we searched all integers between [0 8] based on a previous study that reported 4–8 s latencies in the gray matter [87]. Then the optimal integer was chosen as τ for which the covariance of noise $cov(y(t) - \hat{x}(t) \otimes h(t))$ was smallest, to obtain the set of onsets. Subsequently, the vertex-by-vertex HRF was fitted and extracted with these pseudo-events. The readers are referred to Tagliazucchi et al. [86] and Wu et al. [58] for further details on the deconvolution method.

Supplementary Information

The online version contains supplementary material available at <https://doi.org/10.1186/s40708-021-00150-4>.

Additional file 1: Fig. S1. The importance of performing hemodynamic deconvolution illustrated for two possible scenarios. (a) The BOLD fMRI signals are highly correlated (the bottom left panel), whereas the latent neural signals are not (the top left panel); (b) the underlying latent neural signals are highly synchronized (the top right panel); however, the correlation between the corresponding BOLD fMRI signals are low (the bottom right panel). Both scenarios result from the fact that the HRFs corresponding to the two signals are not the same and have a delay between them. Therefore, when convolved with the latent neural signals, they can introduce or nullify the shifts in the resulting BOLD signal. The (a) scenario can cause false positives, and (b) scenario lead to false negatives.

Acknowledgements

Our special thanks to Krish Sathian, Pennsylvania State University for useful discussions and feedback.

Authors' contributions

GD conceived the study and had a major role in design, data acquisition and writing of the manuscript. YW performed the data analysis to test the hypotheses. JR helped with data acquisition, interpretation of the results and writing of the manuscript.

Funding

This study was supported by the Auburn University MRI Research Center.

Availability of data and materials

The data used in this study will be made available upon reasonable request to the corresponding author.

Declarations

Competing interests

The authors declare that this work was carried out in the absence of any competing interests.

Author details

¹AU MRI Research Center, Department of Electrical & Computer Engineering, Auburn University, 560 Devall Dr, Suite 266D, Auburn, AL 36849, USA. ²Department of Psychological Sciences, Auburn University, Auburn, AL, USA. ³Alabama Advanced Imaging Consortium, Birmingham, AL, USA. ⁴Center for Neuroscience, Auburn University, Auburn, AL, USA. ⁵Key Laboratory for Learning and Cognition, School of Psychology, Capital Normal University, Beijing, China. ⁶Department of Psychiatry, National Institute of Mental Health and Neurosciences, Bangalore, India. ⁷Centre for Brain Research, Indian Institute of Science, Bangalore, India. ⁸Department of Psychiatry, Columbia University, New York, NY, USA.

Received: 9 November 2021 Accepted: 28 December 2021

Published online: 17 January 2022

References

- Mountcastle VB (1997) The columnar organization of the neocortex. *Brain* 120:701–722
- Douglas RJ, Martin KAC (2004) Neuronal circuits of the neocortex. *Annu Rev Neurosci* 27:419–451
- Ferrer I, Fabregues I, Condom E (1986) A Golgi study of the sixth layer of the cerebral cortex. I. The lissencephalic brain of Rodentia, Lagomorpha Insectivora and Chiroptera. *J Anat* 145:217–234
- Gilbert CD (1983) Microcircuitry of the visual cortex. *Annu Rev Neurosci* 6:217–247
- Hubel DH, Wiesel TN (1962) Receptive fields, binocular interaction and functional architecture in the cays visual cortex. *J Physiol* 160:106–154
- Zhang ZW, Deschênes M (1997) Intracortical axonal projections of lamina VI cells of the primary somatosensory cortex in the rat: a single-cell labeling study. *J Neurosci* 17:6365–6379
- Katz LC (1987) Local circuitry of identified projection neurons in cat visual cortex brain slices. *J Neurosci* 7:1223–1249
- Klein A, Tourville J (2012) 101 Labeled brain images and a consistent human cortical labeling protocol. *Front Neurosci* 6:171
- Desikan RS, Ségonne F, Fischl B (2006) An automated labeling system for subdividing the human cerebral cortex on MRI scans into gyral based regions of interest. *Neuroimage* 31:968–980
- Fischl B et al (2004) Automatically parcellating the human cerebral cortex. *Cereb Cortex* 14:11–22
- Destrieux C, Fischl B, Dale A, Halgren E (2010) Automatic parcellation of human cortical gyri and sulci using standard anatomical nomenclature. *Neuroimage* 53:1–15
- Turner R, Geyer S (2014) Comparing like with like: the power of knowing where you are. *Brain Connect* 4:547–557
- Chen G, Wang F, Gore JC, Roe AW (2013) Layer-specific BOLD activation in awake monkey V1 revealed by ultra-high spatial resolution functional magnetic resonance imaging. *Neuroimage* 64:147–155
- Heinzle J, Koopmans PJ, den Ouden HEMM, Raman S, Stephan KE (2016) A hemodynamic model for layered BOLD signals. *Neuroimage* 125:556–570
- Kok P, Bains LJ, Van Mourik T, Norris DG, De Lange FP (2016) Selective activation of the deep layers of the human primary visual cortex by top-down feedback. *Curr Biol* 26:371–376
- Koopmans PJ, Barth M, Orzada S, Norris DG (2011) Multi-echo fMRI of the cortical laminae in humans at 7 T. *Neuroimage* 56:1276–1285
- Koopmans PJ, Orzada S, Barth M, Norris DG (2009) Distinguishing pial and laminar gradient-echo BOLD signals at 7 Tesla. *Proc Int Soc Magn Reson Med* 2009:4064
- Olman CA et al (2012) Layer-specific fmri reflects different neuronal computations at different depths in human V1. *PLoS ONE* 7:e32536
- Muckli L et al (2015) Contextual feedback to superficial layers of V1. *Curr Biol* 25:2690–2695
- Polimeni JR, Fischl B, Greve DN, Wald LL (2010) Laminar-specific output-to input-layer connections between cortical areas V1 and MT observed with high-resolution resting-state fMRI. *Proc Int Soc Magn Reson Med* 18:3471
- Polimeni JR, Fischl B, Greve DN, Wald LL (2010) Laminar analysis of 7T BOLD using an imposed spatial activation pattern in human V1. *Neuroimage* 52:1334–1346
- Koopmans PJ, Barth M, Norris DG (2010) Layer-specific BOLD activation in human V1. *Hum Brain Mapp* 31:1297–1304
- Bandettini P (2012) The BOLD plot thickens: sign-and layer-dependent hemodynamic changes with activation. *Neuron* 76:468–469
- Biswal B, Yetkin FZ, Haughton VM, Hyde JS (1995) Functional connectivity in the motor cortex of resting human brain using echo-planar MRI. *Magn Reson Med* 34:537–541
- Lehmann M et al (2015) Loss of functional connectivity is greater outside the default mode network in nonfamilial early-onset Alzheimer's disease variants. *Neurobiol Aging* 36:2678–2686
- Fernández-Seara MA et al (2015) Resting state functional connectivity of the subthalamic nucleus in Parkinson's disease assessed using arterial spin-labeled perfusion fMRI. *Hum Brain Mapp* 36:1937–1950
- Yu Q et al (2012) Brain connectivity networks in schizophrenia underlying resting state functional magnetic resonance imaging. *Curr Top Med Chem* 12:2415–2425
- Wang K et al (2007) Altered functional connectivity in early Alzheimer's disease: a resting-state fMRI study. *Hum Brain Mapp* 28:967–978
- Brier MR et al (2014) Functional connectivity and graph theory in preclinical Alzheimer's disease. *Neurobiol Aging* 35:757–768
- Plitt M, Barnes KA, Wallace GL, Kenworthy L, Martin A (2015) Resting-state functional connectivity predicts longitudinal change in autistic traits and adaptive functioning in autism. *Proc Natl Acad Sci USA* 112:E6699–E6706
- Jia H, Hu X, Deshpande G (2014) Behavioral relevance of the dynamics of the functional brain connectome. *Brain Connect* 4:741–759
- Dubois XJ (2016) Brain age: a state-of-mind? On the stability of functional connectivity across behavioral states. *J Neurosci* 36:2325–2328
- Koyama MS et al (2011) Resting-state functional connectivity indexes reading competence in children and adults. *J Neurosci* 31:8617–8624

34. Adachi Y et al (2012) Functional connectivity between anatomically unconnected areas is shaped by collective network-level effects in the macaque cortex. *Cereb Cortex* 22:1586–1592
35. van den Heuvel MP et al (2016) Multimodal analysis of cortical chemoarchitecture and macroscale fMRI resting-state functional connectivity. *Hum Brain Mapp* 37:3103–3113
36. Honey CJ et al (2009) Predicting human resting-state functional connectivity from structural connectivity. *Proc Natl Acad Sci* 106:2035–2040
37. Turk E, Scholtens LH, van den Heuvel MP (2016) Cortical chemoarchitecture shapes macroscale effective functional connectivity patterns in macaque cerebral cortex. *Hum Brain Mapp* 37:1856–1865
38. Shen K, Hutchison RM, Bezgin G, Everling S, McIntosh AR (2015) Network structure shapes spontaneous functional connectivity dynamics. *J Neurosci* 35:5579–5588
39. Senden M, Goebel R, Deco G (2012) Structural connectivity allows for multi-threading during rest: the structure of the cortex leads to efficient alternation between resting state exploratory behavior and default mode processing. *Neuroimage* 60:2274–2284
40. Segall JM et al (2012) Correspondence between structure and function in the human brain at rest. *Front Neuroinform* 6:10
41. Rane S, Kose S, Gore JC, Heckers S (2013) Altered functional and structural connectivity in a schizophrenia patient with complete agenesis of the corpus callosum. *Am J Psychiatry* 170:122–123
42. Polimeni JR, Mianciardi M, Keil B, Wald LL (2015) Cortical depth dependence of physiological fluctuations and whole-brain resting-state functional connectivity at 7T. *Proc Int Soc Magn Reson Med* 23:592
43. Vasireddi A, Vazquez A, Whitney D, Fukuda M, Kim S-G (2016) Functional connectivity of resting hemodynamic signals in submillimeter orientation columns of the visual cortex. *Brain Connect*. <https://doi.org/10.1089/brain.2015.0414>
44. Handwerker DA, Ollinger JM, D'Esposito M (2004) Variation of BOLD hemodynamic responses across subjects and brain regions and their effects on statistical analyses. *Neuroimage* 21:1639–1651
45. Aguirre GK, Zarahn E, D'Esposito M (1998) The variability of human, BOLD hemodynamic responses. *Neuroimage* 8:360–369
46. Siero JCW, Petridou N, Hoogduin H, Luijten PR, Ramsey NF (2011) Cortical depth-dependent temporal dynamics of the BOLD response in the human brain. *J Cereb Blood Flow Metab* 31:1999–2008
47. Yu X, Qian C, Chen D, Dodd SJ, Koretsky AP (2014) Deciphering laminar-specific neural inputs with line-scanning fMRI. *Nat Methods* 11:55–58
48. Siero JCW et al (2013) BOLD specificity and dynamics evaluated in humans at 7 T: comparing gradient-echo and spin-echo hemodynamic responses. *PLoS ONE* 8:e54560
49. Tian P et al (2010) Cortical depth-specific microvascular dilation underlies laminar differences in blood oxygenation level-dependent functional MRI signal. *Proc Natl Acad Sci* 107:15246–15251
50. Jin T, Kim S-G (2008) Cortical layer-dependent dynamic blood oxygenation, cerebral blood flow and cerebral blood volume responses during visual stimulation. *Neuroimage* 43:1–9
51. Panchuelo RMS, Schluppeck D, Harmer J, Bowtell R, Francis S (2014) Assessing the spatial precision of SE and GE-BOLD contrast at 7 tesla. *Brain Topogr* 28:62–65
52. Markuerkiaga I, Barth M, Norris DG (2016) A cortical vascular model for examining the specificity of the laminar BOLD signal. *Neuroimage* 132:491–498
53. Chen JE, Glover GH (2015) BOLD fractional contribution to resting-state functional connectivity above 0.1 Hz. *Neuroimage* 107:207–218
54. Deshpande G, Sathian K, Hu X (2010) Effect of hemodynamic variability on Granger causality analysis of fMRI. *Neuroimage* 52:884–896
55. Rangaprakash D, Wu G, Marinazzo D, Hu X, Deshpande G. Impact of undesirable hemodynamic variability on fMRI functional connectivity. *IEEE Trans Biomed Eng*
56. Fischl B (2012) FreeSurfer. *Neuroimage* 62:774–781
57. Lüsebrink F, Wollrab A, Speck O (2013) Cortical thickness determination of the human brain using high resolution 3T and 7T MRI data. *Neuroimage* 70:122–131
58. Wu G-R et al (2013) A blind deconvolution approach to recover effective connectivity brain networks from resting state fMRI data. *Med Image Anal* 17:365–374
59. Rubio-Garrido P, Pérez-De-Manzo F, Porrero C, Galazo MJ, Clascá F (2009) Thalamic input to distal apical dendrites in neocortical layer 1 is massive and highly convergent. *Cereb Cortex* 19:2380–2395
60. Cruikshank S, Ahmed O, Stevens T (2012) Thalamic control of layer 1 circuits in prefrontal cortex. *J Neurosci* 32:17813–17823
61. Kuramoto E et al (2015) Ventral medial nucleus neurons send thalamo-cortical afferents more widely and more preferentially to layer 1 than neurons of the ventral anterior-ventral lateral nuclear complex in the rat. *Cereb Cortex* 25:221–235
62. Lee AJ et al (2015) Canonical organization of layer 1 neuron-led cortical inhibitory and disinhibitory interneuronal circuits. *Cereb cortex* 25:2114–2126
63. Garcia-Munoz M, Arbutnot GW (2015) Basal ganglia—thalamus and the “crowning enigma.” *Front Neural Circuits* 9:71
64. Roth MM et al (2015) Thalamic nuclei convey diverse contextual information to layer 1 of visual cortex. *Nat Neurosci* 19:148
65. Theyel BB, Lee CC, Sherman SM (2010) Specific and nonspecific thalamocortical connectivity in the auditory and somatosensory thalamocortical slices. *NeuroReport* 21:861–864
66. Cruikshank SJ et al (2012) Thalamic control of layer 1 circuits in prefrontal cortex. *J Neurosci* 32:17813–17823
67. Aboitiz F, Montiel J (2003) One hundred million years of interhemispheric communication: the history of the corpus callosum. *Braz J Med Biol Res* 36:409–420
68. Scicchitano F, van Rijn CM, van Luitelaar G (2015) Unilateral and bilateral cortical resection: effects on spike-wave discharges in a genetic absence epilepsy model. *PLoS ONE* 10:e0133594
69. Van Essen DC, Newsome WT, Bixby JL (1982) The pattern of interhemispheric connections and its relationship to extrastriate visual areas in the macaque monkey. *J Neurosci* 2:265–283
70. Felleman DJ, Van Essen DC (1991) Distributed hierarchical processing in the primate cerebral cortex. *Cereb Cortex* 1:1–47
71. Feldmeyer D, Lübke J, Silver RA, Sakmann B (2002) Synaptic connections between layer 4 spiny neuron-layer 2/3 pyramidal cell pairs in juvenile rat barrel cortex: physiology and anatomy of interlaminar signalling within a cortical column. *J Physiol* 538:803–822
72. Sereno MI, Lutti A, Weiskopf N, Dick F (2013) Mapping the human cortical surface by combining quantitative T1 with retinotopy. *Cereb Cortex* 23:2261–2268
73. Trampel R et al (2012) Laminar-specific fingerprints of different sensorimotor areas obtained during imagined and actual finger tapping. *Proc Intl Soc Mag Reson Med* 20:663
74. Jones SE, Buchbinder BR, Aharon I (2000) Three-dimensional mapping of cortical thickness using Laplace's equation. *Hum Brain Mapp* 11:12–32
75. Waehnert MD et al (2014) Anatomically motivated modeling of cortical laminae. *Neuroimage* 93:210–220
76. Barbás H, García-Cabezas MÁ, Zikopoulos B (2013) Frontal-thalamic circuits associated with language. *Brain Lang* 126:49–61
77. Friston KJ, Harrison L, Penny W (2003) Dynamic causal modelling. *Neuroimage* 19:1273–1302
78. Wang Y, Katwal S, Rogers B, Gore J, Deshpande G (2016) Experimental validation of dynamic granger causality for inferring stimulus-evoked sub-100ms timing differences from fMRI. *IEEE Trans Neural Syst Rehabil Eng*. <https://doi.org/10.1109/TNSRE.2016.2593655>
79. Deshpande G, Hu X (2012) Investigating effective brain connectivity from fMRI data: past findings and current issues with reference to Granger causality analysis. *Brain Connect* 2:235–245
80. Deshpande G, Santhanam P, Hu X (2011) Instantaneous and causal connectivity in resting state brain networks derived from functional MRI data. *Neuroimage* 54:1043–1052
81. Deshpande G, LaConte S, James GA, Peltier S, Hu X (2009) Multivariate granger causality analysis of fMRI data. *Hum Brain Mapp* 30:1361–1373
82. Lüsebrink F, Wollrab A, Speck O (2012) Cortical thickness determination of the human brain using high resolution 3T and 7T MRI data. *Neuroimage* 70C:122–131

83. Fischl B et al (2002) Neurotechnique whole brain segmentation: automated labeling of neuroanatomical structures in the human brain. *Neuron* 33:341–355
84. Behrens TEJ et al (2003) Non-invasive mapping of connections between human thalamus and cortex using diffusion imaging. *Nat Neurosci* 6:750–757
85. Greve DN, Fischl B (2009) Accurate and robust brain image alignment using boundary-based registration. *Neuroimage* 48:63–72
86. Tagliazucchi E, Balenzuela P, Fraiman D, Chialvo DR (2012) Criticality in large-scale brain fmri dynamics unveiled by a novel point process analysis. *Front Physiol*. <https://doi.org/10.3389/fphys.2012.00015>
87. Lee AT, Glover GH, Meyer CH (1995) Discrimination of large venous vessels in time-course spiral blood- oxygen-level-dependent magnetic-resonance functional neuroimaging. *Magn Reson Med* 33:745–754

Publisher's Note

Springer Nature remains neutral with regard to jurisdictional claims in published maps and institutional affiliations.

Submit your manuscript to a SpringerOpen[®] journal and benefit from:

- ▶ Convenient online submission
- ▶ Rigorous peer review
- ▶ Open access: articles freely available online
- ▶ High visibility within the field
- ▶ Retaining the copyright to your article

Submit your next manuscript at ▶ [springeropen.com](https://www.springeropen.com)
